Research Square

Preprints are preliminary reports that have not undergone peer review.
They should not be considered conclusive, used to inform clinical practice,
or referenced by the media as validated information.

Neutrophil serine proteases are internalized by glioblastoma cells and modulate cell mechanics, apoptosis, and migration

Alua Shagirova
Nazarbayev University
Maiya Allayarova
Nazarbayev University
Aiya Makhanova
Nazarbayev University
Ruslan Kalendar
Nazarbayev University
Mike-Andrew Westhoff
Ulm University Medical Center
Olena Filchakova
Nazarbayev University
Amanbek Bekturgan
Nazarbayev University
Malika Toleubekova
Nazarbayev University
Anar Ormantayeva
Nazarbayev University
Tri Thanh Pham
Nazarbayev University
Timo Burster
timo.burster@nu.edu.kz

Nazarbayev University

Research Article

Keywords: Neutrophil serine proteases, cathepsin G, neutrophil elastase, glioblastoma cells

Posted Date: November 6th, 2026

DOI: https://doi.org/10.21203/rs.3.rs-10752886/v1

License: This work is licensed under a Creative Commons Attribution 4.0 International License.
Read Full License

Additional Declarations: No competing interests reported.

Abstract

Neutrophil serine proteases (NSPs) are crucial mediators of the immune response, with cathepsin G (CatG) and neutrophil elastase (NE) being prominently released by activated neutrophils during neuroinflammation. Beyond pathogen clearance, NSPs modulate cellular functions through surface binding and internalization. Glioblastoma (GB), the most aggressive primary brain cancer, is characterized by its significant therapeutic resistance and invasive properties. We investigated the effects of CatG and NE on human GB cell lines U87 and A172. Both NSPs were internalized, with NE being mostly sequestered to CD107a+ endocytic compartments. A172 cells were susceptible to NSP-induced apoptosis, whereas U87 cells exhibited resistance. Exposure to CatG or NE significantly reduced cellular stiffness, as revealed by biomechanical profiling via atomic force microscopy (AFM) in U87 and A172 cells, suggesting a protease-mediated transition to a more deformable state. Strikingly, CatG impaired U87 migration, indicating that while softening is often linked to invasion, proteolytic activity may destabilize the structural integrity required for movement. These findings collectively suggest NSP-mediated GB cell plasticity.

Introduction

- Serine proteases function as essential biological regulators whose activity is precisely controlled by endogenous inhibitors known as serpins [1, 2]. During acute inflammatory responses, activated neutrophils release a repertoire of serine proteases, collectively known as neutrophil serine proteases (NSPs), into the extracellular milieu. Key NSPs include neutrophil elastase (NE), the protease proteinase 3 (PR3) which shares the substrate specificity as NE, cathepsin G (CatG), and neutrophil serine protease 4 (NSP4) [3, 4].

Beyond NSPs established extracellular functions in pathogen degradation and matrix remodeling, emerging evidence indicates that NSPs can also modulate cellular behavior through interactions with the cell surface. NSPs can transiently bind to cell surfaces, thereby supporting an immune response. Among these, PR3 and, in particular, CatG and NE are basic proteins and bind electrostatically to the negatively charged sulfate groups of heparan sulfate and chondroitin sulfate proteoglycans [5–8]. In addition to neutrophils, CatG can bind to the cell surface of immune cells and might protect effector $CD8^+$ T cells from “friendly fire”, support intercellular communication between immune cells and target cells by upregulating cell surface MHC I molecules, and arm such cells against viral invasion [9–11]. In addition, the exogenously proteolytically active CatG can be internalized by an EBV-transformed B cell line lacking endogenous CatG expression, subsequently localizing to the endocytic compartment, thereby expanding the panel of proteases involved in antigen processing during inflammation [12]. Furthermore, while CatG shows higher affinity for binding to the cell surface than NE, both NE and CatG, but not PR3, enter cancer cell endosomes via clathrin- and dynamin-dependent endocytosis [13].

Glioblastoma (GB, grade IV astrocytoma) represents the most common and aggressive form of malignant primary brain cancer in adults, characterized by rapid, invasive growth into surrounding

healthy brain tissue, and a poor prognosis with an average survival after diagnosis with standard treatment of approximately 12 to 18 months, even under highly aggressive standard treatment [14]. In general, the glioblastoma cell line A172, classified as proneural, is more prone to apoptosis than the mesenchymal U87 cell line, which exhibits higher migration rates and is highly tumorigenic, reliably generating aggressive tumors when injected into animal models [15].

The role of NE in malignancy is complex, while NE can promote progression by degrading the extracellular matrix [16–18]. While low concentrations of NE (40–80 nM) promote cancer cell proliferation, high concentrations (400 nM) have been shown to kill cancer cells [19]. Later, it was shown that NE (3 µg/ml, approximately 100 nM) selectively kills a panel of cancer cell lines, including A549 and the glioblastoma cell line T98G, and spares non-cancer cells [20].

In the present study, the internalization and functional impact of CatG and NE on U87 and A172 cells were investigated. We show that NSPs induce cell-line-specific apoptosis, significantly alter cellular biomechanics, and hinder cell migration, providing new insights into how neuroinflammation shapes GB cell survival and motility.

Materials and Methods

1. Cells and cell culture

Human glioblastoma cell lines U87 and A172 (ATCC-TCP-1018 Glioma Cell Line Panel, American Type Culture Collection, ATCC, Manassas, VA, USA) and human lung adenocarcinoma epithelial cell line A549 (CCL-185, American Type Culture Collection, ATCC, Manassas, VA, USA) were used in this study.

U87 and A172 cells were maintained in Dulbecco's Modified Eagle Medium (DMEM; Gibco, Thermo Fisher Scientific, Waltham, MA, USA). A549 cells were cultured in RPMI-1640 medium (Sigma-Aldrich, St. Louis, MO, USA). Media was supplemented with 10% heat-inactivated fetal bovine serum (FBS; heat-inactivated at 56°C for 30 min; Gibco, Grand Island, NY, USA) and 1% penicillin–streptomycin (10,000 U/ml penicillin and 10,000 µg/ml streptomycin, pen/strep, Gibco, Thermo Fisher Scientific, Waltham, MA, USA). Cells were maintained at 37°C in a humidified incubator with 5% CO_2. Cells were grown to 80–90% confluency before passaging. After growth, the culture medium from the plates was aspirated, and the cells were washed with prewarmed phosphate-buffered saline (PBS, pH 7.4). Cells were detached using 0.5% trypsin-EDTA (Gibco, Thermo Fisher Scientific, Waltham, MA, USA) and incubated for 5 min at 37°C until detachment was confirmed microscopically. The detached cells were resuspended in complete growth medium and centrifuged at 170 × g for 5 min at room temperature. The supernatant was discarded, and cells were resuspended in fresh complete DMEM for further experiments.

2. Proteases and activity-based probes

Human neutrophil serine proteases (NSPs) were purchased from Athens Research and Technology (Athens, GA, USA). The following enzymes were used: human neutrophil elastase (NE; PN: 16-14-051200, Lot No. EH2024-03) and human cathepsin G (CatG; PN: 16-14-030107, Lot No. CG2024-01).

For activity-based protein profiling, the fluorescence-labeled activity-based probe MARS116-FAM was used for CatG [21], and VPV-FAM was used for NE [22]. The ABPs were kindly provided by Prof. Dr. Marcin Sienczyk and Prof. Dr. Renata Grzywa (Division of Medicinal Chemistry and Microbiology, Faculty of Chemistry, Wroclaw University of Science and Technology, Wroclaw, Poland).

3. Annexin V apoptosis assay by flow cytometry

Apoptosis was assessed using the Cell Meter™ APC-Annexin V Binding Apoptosis Assay Kit (Cat# 22837; AAT Bioquest, Sunnyvale, CA, USA) according to the manufacturer's instructions.

U87 and A172 glioblastoma cells were seeded in 96-well plates one day prior to treatment in complete growth medium (DMEM for A172 and U87, supplemented with 10% FBS and 1% pen/strep). On the day of the experiment, cells were washed and incubated with CatG or NE in a final concentration of 1.5 or 10 µg/ml diluted in serum-free medium for 4 or 16 h. Control samples were incubated in serum-free medium alone. As a positive control for apoptosis induction, staurosporine (Product No. S4400, Sigma-Aldrich, St. Louis, MO, USA) was used at a final concentration of 1 µM. Cells were maintained at 37°C in a humidified atmosphere containing 5% CO_2 for the indicated incubation period. Following treatment, adherent cells were detached using 0.5% trypsin-EDTA, collected, and washed with PBS, pH 7.4. Samples were centrifuged at 170 x g for 5 min, and cell pellets were resuspended in Annexin V binding buffer according to the manufacturer's instructions. Cells were stained with Annexin V reagent and incubated for 15 min at room temperature in the dark. After staining, samples were diluted with binding buffer and immediately analyzed using an Attune NxT Flow Cytometer (Thermo Fisher Scientific, Waltham, MA, United States). Data were processed using FlowJo™ v10.8.1 software (BD Life Sciences, Ashland, OR, USA). The gating strategy included exclusion of debris based on forward scatter (FSC) versus side scatter (SSC), followed by doublet discrimination using FSC-A versus FSC-H. Annexin V-positive cells were considered apoptotic. Statistical analyses were performed using GraphPad Prism v10.6.1. Prior to statistical analysis, data were assessed for normality using the Shapiro-Wilk test. Differences among treatment groups were analyzed separately for each cell line using one-way analysis of variance (ANOVA), followed by Dunnett's multiple-comparisons test to compare each treatment group with the corresponding untreated control. Data are presented as mean ± SD, with individual data points shown where appropriate. Differences were considered statistically significant at $p < 0.05$.

4. Confocal microscopy

U87 and A172 cells were seeded on 8-well glass-bottom slides (Sarstedt, Nümbrecht, Germany) in complete DMEM and incubated for 24 h at 37°C in a humidified atmosphere containing 5% CO_2. In the

case of serum-free conditions, after 24 h, the medium was replaced with serum-free DMEM. CatG or NE in a final concentration of (10 µg/ml) were pre-incubated with the respective activity-based probe (MARS116-FAM for CatG or VPV-FAM for NE, final concentration 0.5 µM) in serum-free medium for 15 min at room temperature in the dark. The resulting protease-ABP complexes were then added to the cells and incubated for 45 min. Following treatment, cells were washed twice with cold PBS, pH 7.4 and fixed with ice-cold 99% methanol for 5 min. After fixation, cells were washed twice with PBS and blocked with PBS containing 10% FBS for 30 min at room temperature.

Cells were incubated with Alexa Fluor® 647-conjugated anti-human CD107a antibody (2 µl, clone H4A3, BioLegend, San Diego, CA, USA) for 1 h at room temperature in the dark. After three washing steps with PBS, nuclei were stained with Hoechst dye (ReadyProbes™ Reagent, Thermo Fisher Scientific, Carlsbad, CA, USA) at a final concentration of 1 µl/ml for 5 min prior to imaging.

Confocal images were acquired using a ZEISS LSM 990 microscope (Carl Zeiss AG, Jena, Germany). Hoechst fluorescence was detected using the DAPI channel (405 nm), ABP-derived fluorescence was detected using the FITC channel (488 nm), and CD107a–Alexa Fluor 647 fluorescence was detected using the 633 nm laser line. Channels were acquired sequentially to prevent spectral overlap. Images were captured using ZEN software (Carl Zeiss AG) and further processed using FIJI software (Schindelin et al., Nat Methods, 2012; updated 2019).

Fluorescence intensity was quantified using corrected total cell fluorescence (CTCF), calculated as:

CTCF = integrated density (area × mean background)

To reduce skewness and stabilize variance, CTCF values were log-transformed using the formula log10(CTCF + 1) prior to statistical analysis. Normality of transformed datasets was evaluated using the Shapiro-Wilk test. Statistical analysis was performed using two-way analysis of variance (ANOVA) with treatment and cell line as fixed factors, followed by Dunnett's multiple-comparisons test to compare each treatment group with the corresponding untreated control within each cell line. Adjusted p-values were calculated for multiple comparisons. Statistical analyses and graph generation were performed using GraphPad Prism v10.6.1. Differences were considered statistically significant at $p < 0.05$.

To evaluate colocalization between FITC-positive signal and CD107a-positive compartments, the FITC and CD107a fluorescence channels were thresholded independently to generate binary masks. Overlapping fluorescence-positive regions were identified using the Image Calculator "AND" operation in Fiji/ImageJ. The overlap area was quantified and normalized to the total FITC-positive area to calculate the percentage overlap. Statistical analyses were performed using GraphPad Prism v10.6.1. Data normality was assessed using the Shapiro-Wilk test. Statistical analysis was performed using two-way analysis of variance (ANOVA) with treatment and cell line as fixed factors, followed by Dunnett's multiple-comparisons test. Differences were considered statistically significant at $p < 0.05$.

5. Atomic force microscopy

Cells were seeded in 30 mm dishes (Corning Inc., Corning, NY, USA) one day prior to treatment in complete growth medium. Before AFM measurements, cells were treated with CatG or NE at final concentrations of 1.5 µg/ml for 4 h. Following treatment, cells were washed three times with PBS (pH 7.4), and AFM measurements were subsequently performed in serum-free medium.

All liquid-phase measurements of A172, U87, and A549 cells were performed using a Bruker NanoWizard 4XP AFM system (Bruker Instruments, Mannheim, Germany) integrated with a Zeiss Observer 7 microscope (Carl Zeiss, Oberkochen, Germany). A biosphere B500-CONT spherical AFM probe composed of diamond-like carbon with a gold coating (nanotools/NanoAndMore) was used for all measurements. The probe had a nominal spring constant of 0.2 N/m and a spherical tip diameter of 1 µm, corresponding to a tip radius of 500 nm. Both probe sensitivity and spring constant were calibrated using a contact-free method. QI™ cells in liquid mode were then performed at a setpoint of 0.5 nN, with a resolution of 1000 nm/pixel and a scan speed of 30 µm/s, to obtain data on the morphological and mechanical properties of cells in media. Data from at least 43 cells per condition were used to calculate the statistical average. The peak height was determined in the JPK Data Processing application by drawing a line along the center of the cell's longitudinal axis to obtain its height profile.

Using the formula given below, the elastic modulus or Young's modulus was calculated by applying a Hertz model to the force-distance curve as follows.

$$F = \frac{4}{3} E^* \sqrt{Rd^3}$$

Where *F* is the applied force, *E** is the effective elastic modulus, *R* is the probe radius, and *d* is the indentation depth. Note that *E** depends on the Poisson's ratio of the sample. The elastic modulus values were obtained from the force-distance curves using the JPK Data Processing software. Prior to curve fitting, the force curves were corrected for tilt and offset, then baseline-fitted. After entering the probe radius and tip geometry, all indentation curves were fitted. The histogram function was then applied to the region corresponding to the cell's peak height to determine the elastic modulus. Statistical significance was evaluated using unpaired *t*-tests for parametric pairs and Mann-Whitney tests for non-parametric pairs in GraphPad Prism 8.4.3.

6. Transwell migration assay

U87 and A172 cells were grown to approximately 90% confluency. On the day of the experiment, cells were trypsinized, centrifuged for 5 min at 170 x g, and the supernatant was aspirated. The cell pellets were washed with serum-free DMEM and centrifuged again for 5 min. Cell migration was assessed using transwell inserts (6.5 mm diameter, 8.0 µm pore size; Costar, Corning Incorporated, NY, USA) placed in 24-well plates. Cells were counted and seeded into the inserts at a density of 2.5 x 10^4 cells per insert. The following conditions were used: control 1 (no attractant), control 2 (with attractant), CatG [1.5 µg/ml], and NE [1.5 µg/ml].

For the first part, cells were maintained in serum-free DMEM in the upper chamber, while the corresponding wells also contained serum-free DMEM. For the CatG- and NE-treated groups, the respective protease was added to both the insert and the lower well. Cells were incubated in this setup for 4 h. This step was needed to ensure equal cell seeding across all conditions and to expose the cells to the active protease before the migration phase. After 4 h, the inserts were transferred to new wells containing DMEM with 10% FBS, which served as a chemoattractant, and incubated for an additional 4 h. The medium in the upper chamber was not replaced, and the chamber remained serum-free. For the no-attractant control, inserts were transferred to wells containing serum-free DMEM for the same period.

After incubation, non-migrated cells were removed from the upper side of the membrane, and the membranes were washed with PBS (pH 7.4). Migrated cells were fixed with ice-cold methanol for 10 min, washed with PBS (pH 7.4) for 10 min, and stained with Hoechst at a final concentration of 10 µg/ml for 30 min in the dark. After staining, membranes were washed again with PBS for 10 min and allowed to dry. Images were acquired using an inverted microscope (ZEISS Axio Vert.A1, Carl Zeiss Microscopy GmbH, Jena, Germany) with the DAPI channel (405 nm). A 10x objective was used, and five images were taken per membrane. Cells were counted in all images, and the mean number of migrated cells per membrane was calculated. For statistical analysis, each condition was normalized to the no-attractant control from the corresponding independent experiment. Data distribution was assessed using the Shapiro-Wilk test. For normally distributed data, one-way ANOVA followed by Tukey's multiple comparisons test was used. For non-normally distributed data, the Kruskal-Wallis test followed by Dunn's multiple-comparisons test was applied. Statistical analysis was performed using GraphPad Prism 8.4.3. For each cell line, four independent experiments were performed (n = 4).

7 Immunofluorescence staining of F-actin

U87 and A172 cells were seeded onto 8-well glass-bottom chamber slides (Sarstedt, Nümbrecht, Germany) in complete DMEM and cultured for 24 h at 37°C in 5% CO_2. For serum-free experiments, the culture medium was replaced with serum-free DMEM after overnight incubation. Cells were treated with CatG or NE at a final concentration of 1.5 µg/ml for 4 h under serum-free conditions. Following treatment, cells were washed twice with PBS and fixed with 4% paraformaldehyde (PFA) for 10–15 min at room temperature. Cells were subsequently washed three times with PBS and permeabilized with 0.1% Triton X-100 in PBS for 10 min at room temperature. After permeabilization, samples were additionally washed three times with PBS and blocked with PBS containing 10% FBS for 30–60 min at room temperature. F-actin was stained using Alexa Fluor 568-conjugated phalloidin (Thermo Fisher Scientific) diluted 1:100 in blocking buffer and incubated for 20–30 min at room temperature in the dark. Afterwards cells were washed three times with PBS. Nuclear counterstaining was performed using Hoechst dye (ReadyProbes™ Reagent, Thermo Fisher Scientific, Carlsbad, CA, USA) at a final concentration of 1 µl/ml for 5 min prior to imaging.

Confocal fluorescence imaging was performed using a ZEISS LSM 980 with Airyscan confocal microscope (Carl Zeiss AG, Jena, Germany). Hoechst fluorescence was detected using the DAPI channel

(405 nm excitation), while Alexa Fluor 568-phalloidin fluorescence was detected using the 561 nm laser. Fluorescence channels were acquired sequentially to minimize spectral overlap. Images were acquired using ZEN software (Carl Zeiss AG) and subsequently processed and analyzed using FIJI/ImageJ software.

8 Live-cell imaging

Live-cell imaging was performed to monitor the intracellular trafficking of ABP complexed with NSPs in real time on 8-well glass-bottom chamber slides (Sarstedt, Nümbrecht, Germany) in complete DMEM. Cells were incubated with ABP complexes under serum-free conditions, and nuclei were counterstained with Hoechst dye immediately before imaging. Time-lapse confocal imaging was performed on ZEISS LSM 980 with Airyscan confocal microscope (Carl Zeiss AG, Jena, Germany). Images were acquired continuously for 1 h using sequential excitation of the DAPI/Hoechst channel (405 nm) and the FITC channel (488 nm). Transmitted-light images were simultaneously recorded with the photomultiplier tube (PMT) detector to visualize cellular morphology and movement. Time-lapse image sequences were acquired using ZEN software (Carl Zeiss AG, Jena, Germany). Three-dimensional reconstruction, visualization, and image analysis were performed using Imaris version 9.9.1 (Bitplane AG, Zurich, Switzerland).

Results

1. Proteolytically active NSPs bind to the surface of U87 and A172 cells and are subsequently internalized

To mimic neuroinflammatory conditions, U87 and A172 cells were incubated with purified CatG or NE. The proteolytic activity of both proteases was tracked using the activity-based probes (ABPs) MARS116-FAM for CatG or VPV-FAM for NE in an approach referred to as activity-based protein profiling. ABPs contain a phosphonate warhead that reacts with the nucleophilic oxygen atom of the active-site serine residue of CatG or NE, forming a covalent bond between the phosphonate and the serine moiety, where the proteolytic activity can be determined by fluorescence microscopy [11]. After initial binding of CatG and NE to the surface of U87 and A172, both NSPs are subsequently internalized (Fig. 1). To further characterize internalization, co-staining with the organelle-specific antibody CD107a (lysosome-associated membrane protein 1, LAMP-1), a marker for endocytic compartments, particularly lysosomes, was performed. Internalization of CatG showed a punctate distribution within the cytoplasm, with comparable CatG uptake in U87 and A172. However, CatG did not co-localize with the CD107a-specific compartment. In contrast, fluorescence signals for NE were more diffuse but significantly co-localized with CD107a, indicating their sequestration within specialized endocytic vesicular structures. Overall, CatG and NE are internalized in U87 and A172 cells, but the proteases localize to different intracellular compartments.

2. The glioblastoma cell line A172 is more susceptible to apoptosis than U87 in a proteolytic environment

In order to ascertain whether CatG and NE induce apoptosis in U87 and A172 cells after internalization, a multiparametric flow cytometric analysis using Annexin V/Propidium Iodide (PI) staining was performed, which differentiates between viable (Annexin V^-/PI^-), early apoptotic (Annexin V^+/PI^-), and late apoptotic (Annexin V^+/PI^+) populations. A172 cells were highly sensitive to both NSPs, showing a significant shift toward apoptosis, particularly after 16 h for CatG (Fig. 2). Conversely, U87 cells maintained high viability, demonstrating resistance to NSP-induced apoptosis. Thus, the findings highlight distinct sensitivity profiles between the two cell lines, with A172 being significantly more responsive to NSPs than U87.

3. Treatment with NSPs reduces the stiffness of U87 and A172

Malignant progression in glioblastoma is driven by both biochemical signals and the physical properties of the cellular microenvironment. The persistent softness of cells is a critical biomechanical marker of high invasiveness and migratory potential [23, 24]. Biomechanical profiling by using atomic force microscopy (AFM) to measure Young's modulus of stiffness (elasticity) was applied to U87 and A172, which were cultured in complete or serum-free (SF, to exclude serine protease inhibitors) media with or without CatG or NE. U87 cells showed significantly higher baseline stiffness than A172 cells (median 2.028 kPa, n = 54 vs. 1.041 kPa, n = 44; p = 0.0011), indicating an intrinsically stiffer mechanical phenotype for U87 cells (Fig. 3 and Supp. Figure 1). Notably, no difference in stiffness was observed between U87 and A549. Culturing cells in SF medium significantly increased stiffness in both cell lines (U87 from 1.971 (n = 54) to 3.083 kPa (n = 54); $p < 0.0001$, and A172 from 1.041 (n = 44) to 1.992 kPa (n = 48); $p < 0.0001$). However, treatment with CatG or NE in SF medium reversed this effect, drastically reducing stiffness (CatG-SF from 2.906 kPa (n = 54) to 0.4906 kPa (n = 43); $p < 0.0001$, and NE-SF from 2.906 kPa (n = 54) to 1.204 kPa (n = 47); $p < 0.0001$). The softening capacity was most pronounced with CatG in U87 cells in SF (0.4906 kPa) and with NE in A172 cells in SF (0.6917 kPa). In conclusion, NSP-mediated transition to a more deformable state alters the physical properties of glioblastoma cell lines, possibly by causing cytoskeletal disintegration.

4. Paradoxical impairment of cell migration by CatG

To investigate whether protease-induced cellular softening correlates with enhanced migrative potential, a Transwell migration assay was performed. Strikingly, CatG and, to a lesser extent, NE (though not to a statistically significant degree) decreased U87 cell transmigration (Fig. 4A), but had no significant effect on A172 cells (Fig. 4B), in which basal migration is already impaired (control). To investigate the direct impact of NSPs on the structural integrity of the actin cytoskeleton of A172, following treatment, cells were fixed and stained with fluorescently labeled phalloidin, a high-affinity probe for filamentous actin (F-actin), to enable precise visualization of the actin cytoskeletal architecture by confocal microscopy. In control cells, F-actin was distributed as well-defined cortical stress fibers and organized peripheral actin

networks, characteristic of adherent cells (Fig. 4C). In contrast, cells exposed to either CatG or NE displayed a loss of actin stress fibers, accompanied by diffuse and fragmented F-actin staining, indicating extensive depolymerization and disassembly of the actin cytoskeleton.

While CatG and NE induce softening in U87 cells, a phenotype often associated with increased invasiveness, the observed reduction in migration suggests that CatG may ultimately lead to cellular detachment. This implies that the resulting biomechanical state could represent structural destabilization or a pre-apoptotic phase that hinders functional motility rather than promoting localized cell migration.

5. Time-dependent uptake of CatG and NE into U87 and A172 cells

U87 and A172 glioblastoma cells were incubated with the fluorescence-labeled activity-based probes MARS116-FAM, for CatG, and VPV-FAM for NE, to enable real-time visualization of active protease localization and internalization within the cells. Following ABP addition, live-cell time-lapse fluorescence microscopy was performed, with images acquired at defined intervals of 0, 15, 30, 45, and 60 minutes to capture the temporal progression of protease uptake and intracellular trafficking (Fig. 5 and supplementary data S2). In parallel with the fluorescence tracking of protease activity, morphological changes in the cells were closely monitored throughout the imaging period. Notably, both U87 and A172 cells exhibited alterations in overall cell shape, including elongation and rounding up, as evidenced by the formation and retraction of membrane protrusions. These morphological responses suggest a potential functional link between extracellular protease activity and cytoskeletal remodeling.

Discussion

GB is characterized by high invasiveness and a complex tumor microenvironment (TME) that supports tumor progression. The infiltration of neutrophils into the TME leads to the release of NSP granule contents, which, in turn, modulate cellular properties and behavior [25]. Our findings indicate that NSPs bind to and enter glioblastoma cell lines, but with different intracellular targets and functional outcomes. CatG is internalized into the cytosol or into CD107a-independent vesicles, and NE is directed mainly toward the endocytic compartment. Whereby U87 cells exhibit resistance to protease-mediated apoptosis. Moreover, A172 glioma cells are inherently more compliant (softer) compared to U87 cells, and exposure to CatG or NE significantly decreases cellular stiffness, with CatG exerting a more prominent effect on U87 cells and NE on A172 cells. However, the migration of U87 cells was significantly impaired due to the activity of CatG, suggesting a potential role in hindering cellular movement.

Understanding changes in Young’s modulus is essential for comprehending how tumor cells navigate and migrate into healthy tissue. While one study reported similar absolute stiffness values for U87 (9.9 ± 1.3 kPa) and A172 (9.6 ± 1.2 kPa) [26], our data highlight a significant baseline gap between both cell lines that is further modulated by the extracellular environment. Serum-free conditions are a relevant

means of mimicking the nutrient-deprived TME as is found in the CNS. The increase in stiffness observed in serum-free medium may represent a stress response or cytoskeletal reorganization during starvation, which serves as a biological "brake" on A172 cell migration but not on U87 cells, where CatG is necessary to suppress cell motility. Excessive protease activity, particularly from CatG, appears to cross a mechanical threshold, causing cytoskeletal disintegration that immobilizes the cell.

In many cancer cells, decreased stiffness is correlated with increased metastatic potential [24]. However, our migration data suggest a more nuanced role for NSPs in GB. CatG-mediated softening was paradoxically associated with decreased migration. This paradox can be explained by the "structural integrity" hypothesis: effective migration requires a balance between deformability and the ability to generate traction force to propel themselves forward through an intact actin cytoskeleton. This is achieved, for instance, through focal adhesions, which allow the cell to anchor to its surroundings and generate the traction needed for movement. If a cell becomes excessively soft due to the complete disintegration of the actin cytoskeleton, the cell loses its structural integrity and cannot produce sufficient tension for movement [24, 27, 28]. Excessive protease activity may lead to cytoskeletal disintegration, rendering the cell too soft to move effectively. Our migration data indicate a more nuanced role for NSPs in U87. CatG-mediated softening was paradoxically linked to decreased migration. This can be explained by the "structural integrity" hypothesis; effective migration requires a balance between deformability and the ability to generate traction force through an intact actin cytoskeleton. The results suggest that excessive protease activity, particularly from CatG, may cross a "softening threshold," leading to cytoskeletal disintegration that hinders functional motility rather than facilitating migration.

U87 cells exhibit resistance to short-term exposure to NSPs, suggesting the presence of cell line-dependent survival mechanisms (Fig. 2). The TRAIL-resistant cell line U87 expresses higher levels of the anti-apoptotic Bcl-2 family member myeloid cell leukemia-1 (Mcl-1) compared to the TRAIL-sensitive A172 [29]. Furthermore, it has been shown that exogenous NE added to cancer cell lines contributes to apoptosis. Indeed, a high concentration of NE (400 nM) is cytotoxic to cancer cells [19], and approximately 100 nM of NE selectively kills the glioblastoma cell line T98G while sparing non-cancer cells [20]. Moreover, a next-generation cytotoxic therapeutic elastase (N17350), designed to selectively kill cancer cells while preserving the immune system, triggers immunogenic cell death (ICD). N17350 is engineered to resist endogenous inhibitors like alpha-1-antitrypsin (A1AT) in the tumor microenvironment, has enhanced enzymatic activity, optimized cell uptake, improved selectivity across a broad range of genetically cancer cells, and minimized off-target toxicity [30]. In the case of CatG (400 nM), detachment-induced cardiomyocyte apoptosis was observed [31].

It has been elucidated that CatG constitutes a key neutrophil component that engages with the tumor cell receptor for advanced glycation end products (RAGE), thereby promoting the recognition and subsequent cytotoxicity toward cancer cells, including Lewis lung carcinoma and the AT3 PYMT breast cancer cell line, in a manner independent of proteolytic activity [32]. Furthermore, a study identifies that CatG induces E-cadherin-dependent aggregation and significantly increases the motility of MCF-7 breast

cancer cells, suggesting an active role in tumor cell dissemination. At low concentrations (2.5-5 nM), this aggregation occurs through a unique cell-oriented mechanism dependent on protease activity rather than just the degradation of the extracellular matrix. In contrast, at higher concentrations (10 nM and above), the extensive degradation of adhesion molecules like fibronectin becomes the primary driver of cell detachment and subsequent aggregation. Unlike NE or trypsin, CatG specifically enhances cell motility and triggers aggregation that potentially modulate cancer metastasis in the tumor microenvironment [33]. As shown in Fig. 2, exogenous CatG and NE induced apoptosis in A172 cells but not in U87 cells, indicating that U87 cells are resistant to neutrophil-mediated cytotoxicity and that CatG impairs the motility of U87.

Severe combined immunodeficiency (SCID) mice lack a functional adaptive immune system, specifically mature T and B cells, while their innate immune defenses are mostly preserved [34]. U87 cells are highly tumorigenic and among the most commonly used models for glioblastoma. When introduced into immunodeficient mice, these cells reliably form vascularized, well-defined tumors [35]. Although the A172 cell line is derived from human glioblastoma and exhibits significant oncogene activation in vitro, it is generally considered non-tumorigenic in immunosuppressed mice [15]. Our data suggest that the preserved innate immune response in models like SCID mice may eliminate sensitive A172 cells via NSP-mediated pathways, while resistant U87 cells evade this defense to establish tumors. This provides one biomechanical explanation for why certain GB cell lines are more tumorigenic in vivo than others.

Neuron-specific γ-enolase (γ-enolase), specifically its C-terminal domain, has neurotrophic-like activity, promoting neuronal survival, differentiation, and regeneration in neurons and glia. γ-enolase participates in accelerated glycolysis, supporting increased tumor cell metabolic demands and proliferation, wherein the C-terminal end of γ-enolase safeguards tumor cells from stressful conditions and therapeutic agents by activating survival-promoting signaling pathways to prevent apoptosis [36]. Glioblastoma cells aberrantly express γ-enolase, which acts as a pro-survival factor supporting tumor cell growth and serves as a primary survival factor under metabolic stress, linked to shorter patient survival [37]. Cathepsin X has been shown to release two amino acids at the C-terminal end of neuron-specific γ-enolase, resulting in reduced neurotrophic activity [38–40]. If cathepsin X cleaves the C-terminal end of γ-enolase and neutralizes these proliferative effects, one would expect that cathepsin X should be absent in more aggressive glioblastoma cells. We showed that cathepsin X is not present in U87 cells, but in A172, T98, and astrocytes, which were cultured in complete medium ([41], supplementary data), indicating that the lack of cathepsin X in U87 might explain why they are more resistant to NSPs-induced apoptosis than A172. On the other hand, cathepsin X was detected in U87 during starvation, grown in 72 h serum-free medium [36]. Hypothetically, cathepsin X could be expressed during starvation in U87 cells and might render them more susceptible to apoptosis.

Conclusions

Our findings suggest that while protease-mediated softening may align with the biomechanical markers of invasion, its functional impact is more related to cellular structural disintegration. This supports the

hypothesis that CatG and NE activity may drive the cells toward a pre-apoptotic state or a softening threshold that weakens the structural integrity needed for active migration. Consequently, while cellular softness remains an important indicator of malignancy, specific protease-mediated pathways, especially involving CatG, may act as a regulatory brake on migration by destabilizing the cellular machinery necessary for movement. Indeed, a softening threshold could be used therapeutically; inducing excessive softening might be a strategy to immobilize tumor cells. Further investigation of the tumor microenvironment and NSP mimetics or activators could lead to new drugs that exploit these mechanisms to combat glioblastoma effectively.

Declarations

Conflict of Interest

The authors declare that the research was conducted in the absence of any commercial or financial relationships that could be construed as a potential conflict of interest.

Funding

This research was funded by the Nazarbayev University Collaborative Research Grant, project number: 20122022CRP1615, and the Committee of Science of the Ministry of Science and Higher Education of the Republic of Kazakhstan (grant no. AP23483529).

Author Contribution

Conceptualization, T.B.; methodology, A.S., M.A., A.M., O.F., A.B., M.T., A.O., and T.T.P.; software, R.K..; validation, R.K., M.A.W., T.T.P., and T.B.; formal analysis, A.S., M.A., M.A.W., T.T.P., and T.B.; investigation, A.S., M.A., A.M., O.F., A.B., M.T., A.O., and T.T.P.; writing, T.B.; review and editing, A.S., M.A., A.M., R.K., M.A.W., O.F., A.B., M.T., A.O., and T.T.P..; supervision, T.B.; project administration, T.B.; funding acquisition, T.B. All authors have read and agreed to the published version of the manuscript.

Acknowledgement

We thank Prof. Dr. Marcin Sienczyk and Prof. Dr. Renata Grzywa (Division of Medicinal Chemistry and Microbiology, Faculty of Chemistry, Wroclaw University of Technology, Wroclaw, Poland) for the activity-based probes MARS116-FAM and VPV-FAM.

References

1. Kahler JP, Vanhoutte R, Verhelst SHL. Activity-Based Protein Profiling of Serine Proteases in Immune Cells. Arch Immunol Ther Exp (Warsz). 2020;68(4):23.
2. Di Cera E. Serine proteases. IUBMB Life. 2009;61(5):510–5.
3. Burster T, Gartner F, Knippschild U, Zhanapiya A. Activity-Based Probes to Utilize the Proteolytic Activity of Cathepsin G in Biological Samples. Front Chem. 2021;9:628295.
4. Kasperkiewicz P, Poreba M, Groborz K, Drag M. Emerging challenges in the design of selective substrates, inhibitors and activity-based probes for indistinguishable proteases. FEBS J. 2017;284(10):1518–39.
5. Campbell EJ, Owen CA. The sulfate groups of chondroitin sulfate- and heparan sulfate-containing proteoglycans in neutrophil plasma membranes are novel binding sites for human leukocyte elastase and cathepsin G. J Biol Chem. 2007;282(19):14645–54.
6. Burster T, Mustafa Z, Myrzakhmetova D, Zhanapiya A, Zimecki M. Hindrance of the Proteolytic Activity of Neutrophil-Derived Serine Proteases by Serine Protease Inhibitors as a Management of Cardiovascular Diseases and Chronic Inflammation. Front Chem. 2021;9:784003.
7. Owen CA, Campbell MA, Sannes PL, Boukedes SS, Campbell EJ. Cell surface-bound elastase and cathepsin G on human neutrophils: a novel, non-oxidative mechanism by which neutrophils focus and preserve catalytic activity of serine proteinases. J Cell Biol. 1995;131(3):775–89.
8. Owen CA, Campbell MA, Boukedes SS, Campbell EJ. Inducible binding of bioactive cathepsin G to the cell surface of neutrophils. A novel mechanism for mediating extracellular catalytic activity of cathepsin G. J Immunol. 1995;155(12):5803–10.
9. Burster T, Knippschild U, Molnar F, Zhanapiya A. Cathepsin G and its Dichotomous Role in Modulating Levels of MHC Class I Molecules. Arch Immunol Ther Exp (Warsz). 2020;68(4):25.
10. Delgado MB, Clark-Lewis I, Loetscher P, Langen H, Thelen M, Baggiolini M, Wolf M. Rapid inactivation of stromal cell-derived factor-1 by cathepsin G associated with lymphocytes. Eur J Immunol. 2001;31(3):699–707.
11. Assylbekova A, Allayarova M, Konysbekova M, Bekturgan A, Makhanova A, Brown S, Grzegorzek N, Kalbacher H, Kalendar R, Burster T. The Proteolytic Activity of Neutrophil-Derived Serine Proteases Bound to the Cell Surface Arming Lung Epithelial Cells for Viral Defense. *Molecules* 2024, 29(18).
12. Burster T, Beck A, Tolosa E, Marin-Esteban V, Rotzschke O, Falk K, Lautwein A, Reich M, Brandenburg J, Schwarz G, et al. Cathepsin G, and not the asparagine-specific endoprotease, controls the processing of myelin basic protein in lysosomes from human B lymphocytes. J Immunol. 2004;172(9):5495–503.
13. Gregory AD, Hale P, Perlmutter DH, Houghton AM. Clathrin pit-mediated endocytosis of neutrophil elastase and cathepsin G by cancer cells. J Biol Chem. 2012;287(42):35341–50.
14. Durga YK, Pusapati RV. Drug resistance in glioblastoma: Challenges, mechanisms and therapeutic strategies (Review). Mol Clin Oncol. 2026;24(1):4.
15. de Ridder LI, Laerum OD, Mork SJ, Bigner DD. Invasiveness of human glioma cell lines in vitro: relation to tumorigenicity in athymic mice. Acta Neuropathol. 1987;72(3):207–13.

16. Akizuki M, Fukutomi T, Takasugi M, Takahashi S, Sato T, Harao M, Mizumoto T, Yamashita J. Prognostic significance of immunoreactive neutrophil elastase in human breast cancer: long-term follow-up results in 313 patients. Neoplasia. 2007;9(3):260–4.
17. Sun Z, Yang P. Role of imbalance between neutrophil elastase and alpha 1-antitrypsin in cancer development and progression. Lancet Oncol. 2004;5(3):182–90.
18. Deryugina E, Carre A, Ardi V, Muramatsu T, Schmidt J, Pham C, Quigley JP. Neutrophil Elastase Facilitates Tumor Cell Intravasation and Early Metastatic Events. *iScience* 2020, 23(12):101799.
19. Houghton AM, Rzymkiewicz DM, Ji H, Gregory AD, Egea EE, Metz HE, Stolz DB, Land SR, Marconcini LA, Kliment CR, et al. Neutrophil elastase-mediated degradation of IRS-1 accelerates lung tumor growth. Nat Med. 2010;16(2):219–23.
20. Cui C, Chakraborty K, Tang XA, Zhou G, Schoenfelt KQ, Becker KM, Hoffman A, Chang YF, Blank A, Reardon CA, et al. Neutrophil elastase selectively kills cancer cells and attenuates tumorigenesis. Cell. 2021;184(12):3163–e31773121.
21. Zou F, Schmon M, Sienczyk M, Grzywa R, Palesch D, Boehm BO, Sun ZL, Watts C, Schirmbeck R, Burster T. Application of a novel highly sensitive activity-based probe for detection of cathepsin G. Anal Biochem. 2012;421(2):667–72.
22. Grzywa R, Burchacka E, Lecka M, Winiarski L, Walczak M, Lupicka-Slowik A, Wysocka M, Burster T, Bobrek K, Csencsits-Smith K, et al. Synthesis of novel phosphonic-type activity-based probes for neutrophil serine proteases and their application in spleen lysates of different organisms. ChemBioChem. 2014;15(17):2605–12.
23. Masud N, Hasib MHH, Ibironke B, Block C, Hughes J, Ekpenyong A, Sarkar A. Exploring the heterogeneity in glioblastoma cellular mechanics using in-vitro assays and atomic force microscopy. Sci Rep. 2025;15(1):19302.
24. Luo Q, Kuang D, Zhang B, Song G. Cell stiffness determined by atomic force microscopy and its correlation with cell motility. Biochim Biophys Acta. 2016;1860(9):1953–60.
25. Rawat K, Syeda S, Shrivastava A. Neutrophil-derived granule cargoes: paving the way for tumor growth and progression. Cancer Metastasis Rev. 2021;40(1):221–44.
26. Louca M, Stylianou A, Minia A, Pliaka V, Alexopoulos LG, Gkretsi V, Stylianopoulos T. Ras suppressor-1 (RSU-1) promotes cell invasion in aggressive glioma cells and inhibits it in non-aggressive cells through STAT6 phospho-regulation. Sci Rep. 2019;9(1):7782.
27. Tang DD, Gerlach BD. The roles and regulation of the actin cytoskeleton, intermediate filaments and microtubules in smooth muscle cell migration. Respir Res. 2017;18(1):54.
28. Westhoff MA, Zhou S, Nonnenmacher L, Karpel-Massler G, Jennewein C, Schneider M, Halatsch ME, Carragher NO, Baumann B, Krause A, et al. Inhibition of NF-kappaB signaling ablates the invasive phenotype of glioblastoma. Mol Cancer Res. 2013;11(12):1611–23.
29. Murphy AC, Weyhenmeyer B, Noonan J, Kilbride SM, Schimansky S, Loh KP, Kogel D, Letai AG, Prehn JH, Murphy BM. Modulation of Mcl-1 sensitizes glioblastoma to TRAIL-induced apoptosis. Apoptosis. 2014;19(4):629–42.

30. Gujar R, Cui C, Fumagalli M, Martinez N, Bahador A, Algazi A, Harrington K, Turner C, Becker L. Developing a therapeutic elastase that stimulates anti-tumor immunity by selectively killing cancer cells. Cell Rep Med. 2025;6(11):102446.
31. Sabri A, Alcott SG, Elouardighi H, Pak E, Derian C, Andrade-Gordon P, Kinnally K, Steinberg SF. Neutrophil cathepsin G promotes detachment-induced cardiomyocyte apoptosis via a protease-activated receptor-independent mechanism. J Biol Chem. 2003;278(26):23944–54.
32. Sionov RV, Fainsod-Levi T, Zelter T, Polyansky L, Pham CT, Granot Z. Neutrophil Cathepsin G and Tumor Cell RAGE Facilitate Neutrophil Anti-Tumor Cytotoxicity. Oncoimmunology. 2019;8(9):e1624129.
33. Yui S, Osawa Y, Ichisugi T, Morimoto-Kamata R. Neutrophil cathepsin G, but not elastase, induces aggregation of MCF-7 mammary carcinoma cells by a protease activity-dependent cell-oriented mechanism. Mediators Inflamm. 2014;2014:971409.
34. Zhang B, Duan Z, Zhao Y. Mouse models with human immunity and their application in biomedical research. J Cell Mol Med. 2009;13(6):1043–58.
35. Candolfi M, Curtin JF, Nichols WS, Muhammad AG, King GD, Pluhar GE, McNiel EA, Ohlfest JR, Freese AB, Moore PF, et al. Intracranial glioblastoma models in preclinical neuro-oncology: neuropathological characterization and tumor progression. J Neurooncol. 2007;85(2):133–48.
36. Vizin T, Kos J. Gamma-enolase: a well-known tumour marker, with a less-known role in cancer. Radiol Oncol. 2015;49(3):217–26.
37. Yan T, Skaftnesmo KO, Leiss L, Sleire L, Wang J, Li X, Enger PO. Neuronal markers are expressed in human gliomas and NSE knockdown sensitizes glioblastoma cells to radiotherapy and temozolomide. BMC Cancer. 2011;11:524.
38. Horvat S, Kos J, Pislar A. Multifunctional roles of gamma-enolase in the central nervous system: more than a neuronal marker. Cell Biosci. 2024;14(1):61.
39. Horvat S, Fonovic UP, Mitrovic A, Zidar N, Kos J, Pislar A. The alpha- to gamma-enolase switch: The role and regulation of gamma-enolase during oligodendrocyte differentiation. Int J Biol Macromol. 2025;301:140464.
40. Obermajer N, Doljak B, Jamnik P, Fonovic UP, Kos J. Cathepsin X cleaves the C-terminal dipeptide of alpha- and gamma-enolase and impairs survival and neuritogenesis of neuronal cells. Int J Biochem Cell Biol. 2009;41(8–9):1685–96.
41. Palesch D, Wagner J, Meid A, Molenda N, Sienczyk M, Burkhardt J, Munch J, Prokop L, Stevanovic S, Westhoff MA, et al. Cathepsin G-mediated proteolytic degradation of MHC class I molecules to facilitate immune detection of human glioblastoma cells. Cancer Immunol Immunother. 2016;65(3):283–91.

Figures

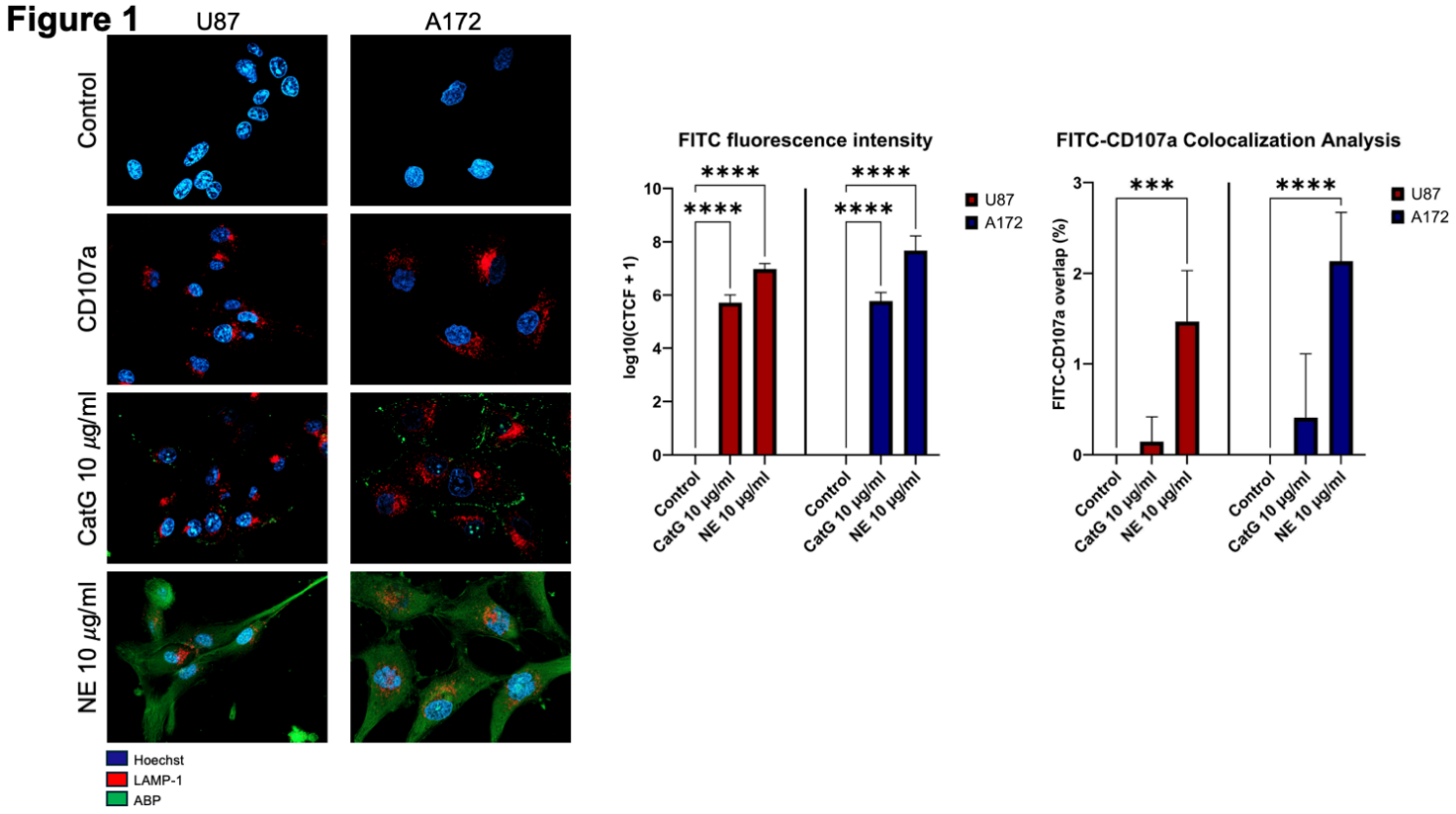
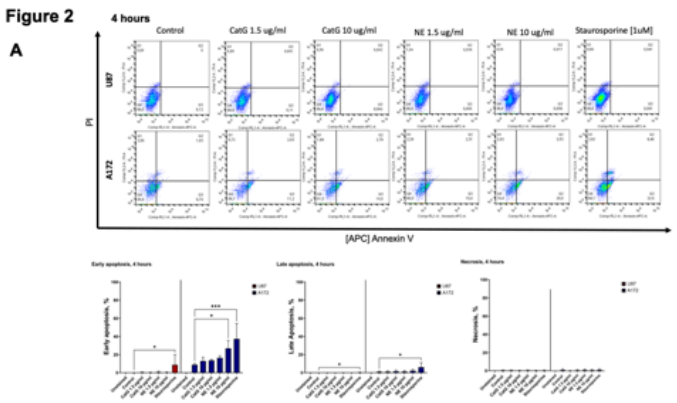


Figure 1

Internalization and subcellular localization of proteolytically active CatG and NE in U87 and A172 cells. U87 and A172 cells were incubated with purified CatG or NE, and their proteolytic activity was tracked using activity-based probes (ABPs) MARS116-FAM for CatG or VPV-FAM for NE. Co-staining with the lysosomal marker CD107a (LAMP-1) was used to reveal distinct subcellular localizations (left panel). Quantitative analysis of FITC fluorescence intensity demonstrated significant uptake of active proteases in both U87 and A172 cells. Colocalization analysis revealed increased overlap between NE-associated fluorescence and CD107a-positive lysosomal compartments compared to CatG (right panel). Data are presented as mean ± SD, n = 4. Statistical significance was determined using two-way ANOVA with multiple comparisons. *** $p < 0.001$, **** $p < 0.0001$.



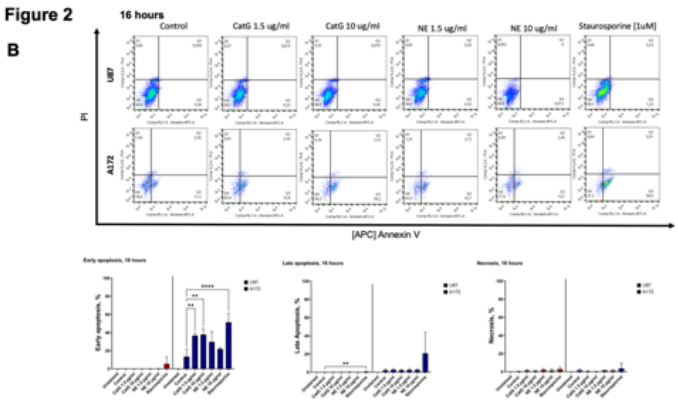


Figure 2

Flow cytometric analysis of apoptosis. (A) Representative dot plots of Annexin V-APC/PI staining for U87 and A172 cells treated with CatG or NE (1.5 µg/ml or 10 µg/ml) in serum-free medium for 4 h and (B) for 16 h. Staurosporine (1 µM) was included as a positive control for apoptosis induction. (C) Bar graphs summarizing early apoptosis, late apoptosis, and necrosis after 4 h, and (D) after 16 h. Data are presented as mean ± SD (n = 4 for the 4 h experiments and n = 3 for the 16 h experiments). Statistical significance was determined separately for both cell lines (U87 and A172) using one-way ANOVA followed by Dunnett's multiple comparisons test. ** p < 0.01, *** p < 0.001, **** p < 0.0001.

Figure 3

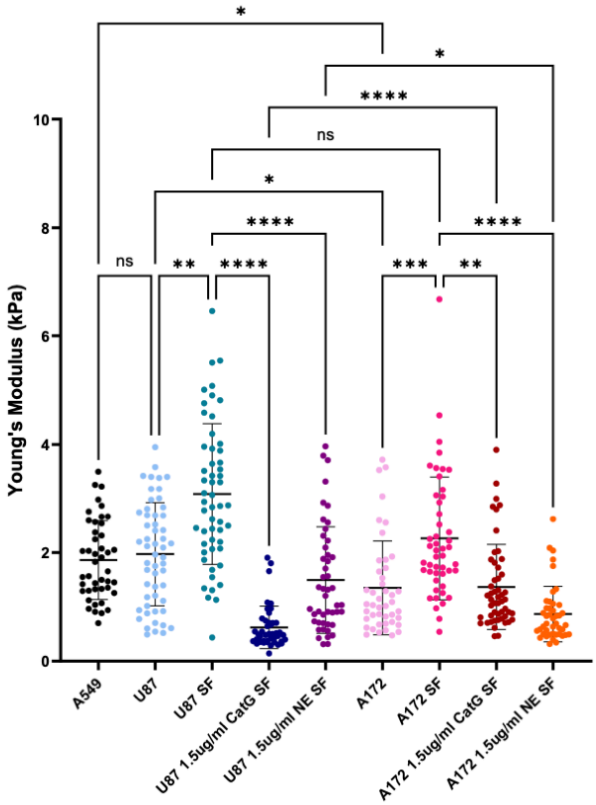


Figure 3

Biomechanical Profiling. Young’s modulus measurements comparing U87, A172, and A549 cells under control, serum-free medium, and protease-treated conditions. Biomechanical profiling using atomic force microscopy (AFM) was performed to measure the Young's modulus of stiffness in U87 and A172 cells.

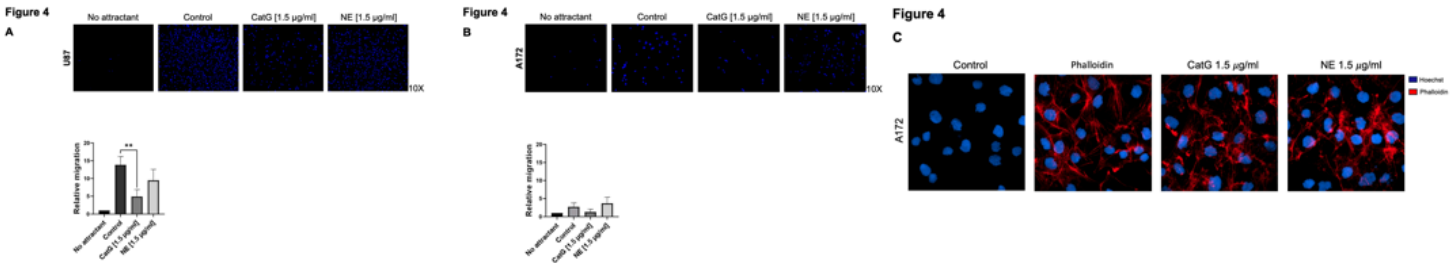
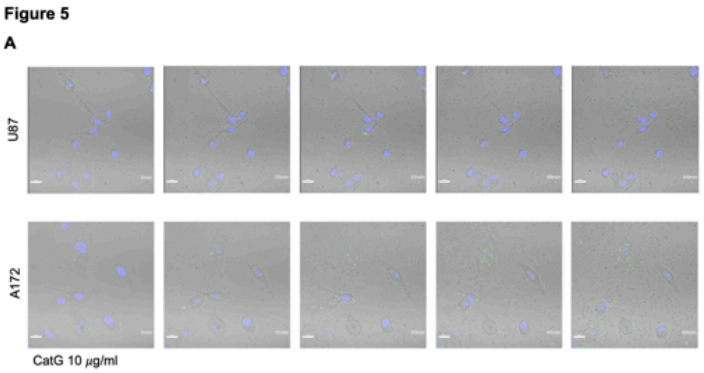


Figure 4

CatG and NE differentially affect transwell migration of U87 and A172 cells. Representative images of Hoechst-stained migrated cells and quantification of relative migration are shown for U87 (A) and A172 cells (B). Cells were pre-incubated for 4 h under serum-free conditions in the absence or presence of CatG or NE [1.5 µg/ml], followed by transfer of the inserts to wells containing 10% FBS for an additional 4 h. A no-attractant control was maintained in serum-free DMEM. Migrated cells were imaged at 10x magnification and quantified from five fields per membrane. Values were normalized to the no-attractant control for each independent experiment. Data are presented as mean ± SD, n = 4. U87 data were analyzed by one-way ANOVA with Tukey's multiple comparisons test, and A172 data by Kruskal-Wallis test with Dunn's multiple-comparisons test, $p < 0.01$ (**).

C) CatG and NE induce distinct actin cytoskeletal rearrangements in glioblastoma cells. Representative confocal images of A172 cells stained with phalloidin to visualize F-actin (red) after treatment with CatG or NE [1.5 µg/ml] under serum-free conditions for 4 h. Nuclei were counterstained with Hoechst (blue), n=3.



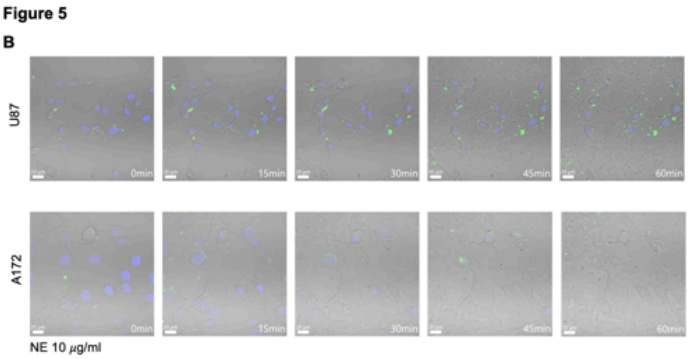


Figure 5

Time-dependent morphological dynamics of U87 and A172 cells following protease treatment. Representative live-cell time-lapse images of U87 cells acquired at 0, 15, 30, 45, and 60 min. Sequential imaging demonstrates dynamic alterations in cellular morphology over time, including changes in cell shape, elongation, and membrane protrusive activity. Images are representative of independent experiments, n=2.

Supplementary Files

This is a list of supplementary files associated with this preprint. Click to download.

- Supp1.tiff
- Supp2A.tiff

- Supp2B.tiff